The Effects of Random Errors in Rawinsonde Data on Derived Kinematic Quantities

CAROL L. BELT[1] AND HENRY E. FUELBERG

Department of Earth and Atmospheric Sciences, Saint Louis University, St. Louis, MO 63103

(Manuscript received 4 August 1981, in final form 12 November 1981)

ABSTRACT

An analysis is conducted to assess the sensitivity of kinematic parameters to random errors contained in rawinsonde data. Parameters considered are relative vorticity, vorticity advection, horizontal divergence, kinematic vertical motion and temperature advection. Input data are from the AVE-SESAME I experiment which coincides with the Red River Valley tornado outbreak (10–11 April 1979). National Weather Service rawinsonde data describe the effects of data errors on the synoptic scale, while the addition of 16 special sites permits a description of sensitivity on the meso-α scale.

Qualitative and quantitative analyses show that horizontal divergence is the most affected of the parameters studied, while vorticity advection ranks second. At 850, 500 and 300 mb, assumed data errors do not preclude detection of the major forcing processes associated with the tornado outbreak. Although the two scales of analysis respond somewhat differently to the data perturbations, fields from both sets of data usually show the same major features.

1. Introduction

Many atmospheric phenomena are investigated using kinematic quantities which are derived from rawinsonde data. Rawinsonde data have been shown, however, to be plagued by systematic and random errors (Kurihara, 1961). Objective analysis and smoothing procedures reduce the effects of data errors (e.g., Barnes, 1964; O'Brien, 1970; Shuman, 1957); however, they do not totally remove the problem. This poses a question: how much confidence can we place on derived kinematic values? This paper seeks to answer that question.

There are at least two popular procedures for determining the effects of rawinsonde data errors on computational results: 1) an error propagation method, which uses equations to describe sensitivity of the final product in terms of original data uncertainty (e.g., Chen and Bosart, 1977; Dupuis and Scoggins, 1979); and 2) a random error method, in which errors are introduced into the data prior to computation with results compared to those from original data (e.g., Fuelberg and Scoggins, 1980; Vincent and Chang, 1975; Ward and Smith, 1976). The latter technique was chosen for this study because, unlike the error propagation method, it more easily allows the incorporation of smoothing schemes and objective data analyses. These processes are desirable since they reduce the impact of errors on computational results. Although the random error method has been widely used in kinetic energy studies, published results of its use in kinematic analyses are rare.

The purpose of this paper is to examine the effects of random errors on kinematic quantities often used in meteorological studies. Both synoptic and subsynoptic (meso α) scale rawinsonde data are used in an attempt to determine differences in resolution and, simultaneously, assess confidence limits in the parameters at each scale. Kinematic quantities under consideration are relative vorticity, vorticity advection, horizontal divergence, kinematic vertical motion and temperature advection. For expediency, qualitative results are discussed in terms of levels most often used by the practicing forecaster: 850 mb and 300 mb for lower- and upper-level horizontal divergence, respectively, and 500 mb for the remainder of the parameters.

2. Methodology

a. Data

Data from the first Atmospheric Variability Experiment-Severe Environmental Storms and Mesoscale Experiment (AVE-SESAME I) conducted on 10–11 April 1979 were used in this study (Gerhard *et al.*, 1979). Specifically, data from 2100 GMT 10 April were selected because preliminary results indicated well-developed kinematic features, little missing data, and because it coincided with the beginning of the Red River Valley tornado outbreak. Twenty-three National Weather Service (NWS) and

[1] Captain, U.S. Air Force.

0027-0644/82/020091-11$06.75

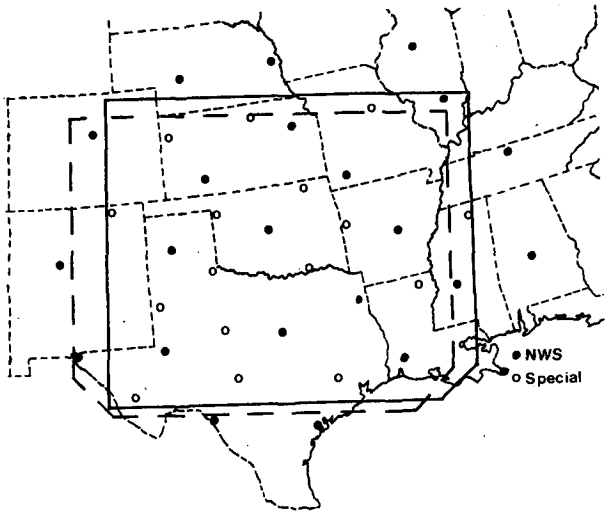

FIG. 1. Rawinsonde stations participating in AVE-SESAME I. The dashed line encloses the area of statistical comparison used with synoptic-scale data while the solid line encompasses the area of subsynoptic-scale data comparison.

16 special rawinsonde stations participated in the experiment (Fig. 1). The NWS stations alone, having an average station spacing of 400 km, provide standard synoptic-scale resolution, but the combination of NWS and special site stations, having an average spacing of 250 km, yields meso α (subsynoptic)-scale resolution. Further details about the AVE-SESAME '79 experiments are given by Alberty *et al.* (1979) and Hill *et al.* (1979).

b. Synoptic situation

Since a complete description of synoptic conditions during the period is given by Moore and Fuelberg (1981), only highlights for 2100 GMT are given here (Fig. 2). The surface pattern (Fig. 2a) is dominated by a low centered over the Colorado-New Mexico border. A cold front extends southward along the Texas-New Mexico border, while a warm front reaches southeastward through north central Texas and into Louisiana. A dry line stretches from the southern Texas panhandle into the Big Bend region (not shown). At 850 mb (Fig. 2b), a low-level southerly jet containing speeds up to 23 m s^{-1} is located over northeastern Texas. Jet intrusion from the southwest is evident at 300 mb (Fig. 2c). Also at 300 mb, a limited jet maximum with winds up to 65 m s^{-1} is centered over Oklahoma. It is noteworthy that this wind maximum tripled in speed during the previous 3 h time period. The radar summary (Fig. 2a) reveals the most intense convective activity occurring in the Red River Valley of Texas and Oklahoma, producing tops to 48 000 ft (14.6 km). The majority of Oklahoma and the Texas panhandle is covered by an extension of this activity. The Wichita Falls tornado touched down at 0000 GMT 11 April.

c. Analytical procedures

Wind data at the various stations were filtered over 50 mb layers to reduce the effects of errors. Filtered values were arithmetic averages of the data at the central level and the levels lying 25 mb on either side. All data then were converted to a gridded format through use of the Barnes objective analysis scheme (Barnes, 1964). The synoptic-scale data set (NWS stations alone) was placed on a 14 × 14 grid

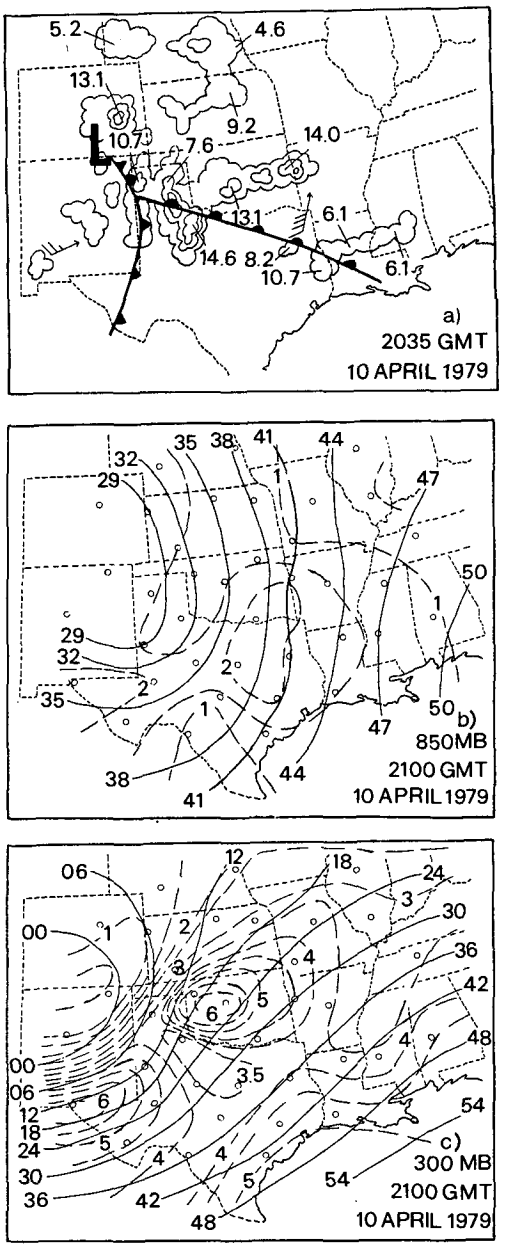

FIG. 2. Radar summary for 2035 GMT 10 April 1979 (echo tops in kilometers). Surface fronts and upper-level maps are for 2100 GMT. Dashed lines at 850 and 300 mb are isotachs (2 = 20 m s^{-1}). At 850 mb, 38 means 1380 m while at 300 mb, 06 means 9060 m.

with 158 km grid spacing. A scan radius of 537 km (3.4 grid intervals) together with four iterations was employed. Subsynoptic-scale data (NWS plus special sites) were placed on a 15 × 13 grid with 127 km spacing. In this case, the scan radius was 381 km (3 grid intervals), and four iterations were used. Although grids from both data sets appeared quite reasonable to the eye, a very mild filter (Shuman, 1957) was applied in both cases to suppress any spurious waves that were not apparent. The smoothing element index was 0.1.

Based on information contained in the Barnes (1964) report, response curves describing the gridded fields at both scales were prepared (Fig. 3). Effects of the Shuman filter are included; however, the figure does not include the additional 50 mb vertical filter applied to the winds. A goal of the objective analysis was to greatly reduce features having wavelengths less than twice the station spacing. This is desirable because "noise" generated by random data errors are manifested at the smaller wavelengths. Also, smaller features are not adequately resolved by the available data. Fig. 3 shows that the addition of the 16 special sites provides considerably better resolution of phenomena having wavelengths of ~750 km.

Gridded data were prepared at the surface and at 50 mb intervals from 900 to 100 mb, producing a total of 18 levels. Centered finite differences were used to compute the space derivatives in the divergence, vorticity and advection terms. The kinematic

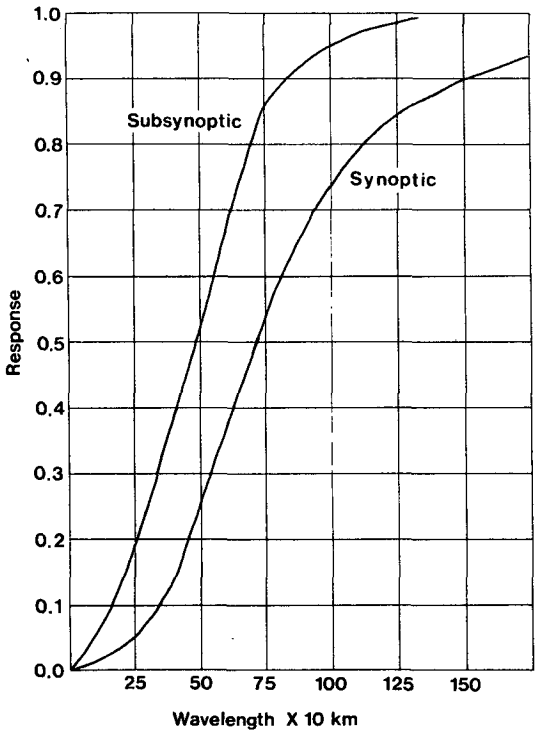

FIG. 3. Response curves for gridded data fields.

TABLE 1. Standard deviations of normally distributed perturbations applied to station data.

Pressure level (mb)	Wind direction (deg)	Wind speed (m s^{-1})
100	15.0	5.6
200	12.7	5.1
300	10.6	4.5
500	6.2	3.4
700	4.0	2.2
900	2.0	1.1

method was used to obtain vertical motion. Vertical motion at the surface was assumed to be zero when using synoptic-scale data, but equaled dp_s/dt when the subsynoptic-scale data were employed. In the latter case, the effects of surface pressure tendency, cross-isobaric flow and terrain were considered; however, their combined effects generally were <1 μb s^{-1}, except over mountainous terrain. Values of ω were assumed to be zero at 100 mb for both data sets by applying the O'Brien (1970) adjustment scheme. For consistency with ω, divergence was adjusted using a scheme by O'Brien in which the modifications were a linear function of pressure.

d. Error simulation

Fields of the kinematic quantities under investigation were computed at each of the 18 levels, using the gridded station data. Computer-generated random errors were then introduced into the station soundings at 25 mb intervals. These perturbations were normally distributed about zero, with standard deviations a function of pressure. One should note that perturbations of two or more standard deviations are possible since a normal distribution was assumed. Perturbations for wind data (selected levels shown in Table 1) are comparable to those suggested by Kurihara (1961) and used by Ward and Smith (1976), Chen and Bosart (1977), Robertson and Smith (1980) and Fuelberg and Scoggins (1980). Middle- and upper-level winds were strong on this day, and the values shown in Table 1 for 500, 300 and 200 mb range from 12–14% of the mean wind speeds at 2100 GMT. A standard deviation of 0.35°C was used at all levels for temperature perturbations (Lenhard, 1970; Hodge and Harmantas, 1965).

Ten sets of perturbed data, each with a different combination of errors, were produced at each of the two data scales. For the ten sets of subsynoptic-scale data, errors at the NWS sites were not the same as those employed for the ten versions of synoptic-scale data (NWS stations only). Although the random perturbations were taken from a population whose mean was zero, the average of perturbations used for specific parameters at particular levels might not be exactly zero. Similarly, non-zero mean errors also

TABLE 2. Statistics on relative vorticity (10^{-6} s^{-1}) for the original and 10 perturbed fields computed from both synoptic (S)- and subsynoptic (Sub)- scale data.

Level (mb)	Data scale	Range of values for the 10 perturbed runs			
		Maximum deviation	Standard deviation	Mean deviation	Correlation coefficient
850	S	5.4–9.2	1.9–3.2	1.6–2.7	0.994–0.998
	Sub	6.6–14.6	2.5–4.7	2.0–3.8	0.987–0.996
700	S	7.7–14.6	2.9–5.0	2.4–3.9	0.989–0.996
	Sub	10.9–19.0	4.1–7.4	3.2–6.1	0.969–0.990
500	S	7.9–22.4	3.8–9.3	3.3–8.2	0.976–0.996
	Sub	19.8–33.5	6.9–11.0	5.2–9.1	0.968–0.987
300	S	15.9–48.5	6.3–18.0	4.9–13.5	0.941–0.993
	Sub	37.6–70.5	16.2–23.0	12.5–17.9	0.930–0.966
200	S	34.8–81.3	13.4–25.4	10.3–20.7	0.673–0.914
	Sub	44.5–92.0	16.2–34.9	12.8–27.5	0.757–0.933

could be expected in sets of only 23 or 39 rawinsonde observations. Gridded fields were obtained of the perturbed data, and kinematic fields then were recalculated using the computational procedures applied to the original data. The effects of systematic data errors and computational inadequacies, such as truncation error, were not considered in this approach.

It is informative to describe effects of the objective analysis and vertical smoothing procedures on the input perturbations of temperature and wind. These schemes treat introduced errors at the stations as waves and therefore reduce portions of them. Standard deviations between the original and perturbed temperature grids were found to be ~0.25°C instead of the 0.35°C that was inserted at the stations. This represents approximately a 70% retention of introduced error. Because wind data were subjected to additional vertical filtering before objective analysis, standard deviations of grid point errors were ~50% of the station values given in Table 1. These reductions in error should not be considered self-defeating to the purposes of the study. Instead, they represent the ability of the computational procedures to filter and partially remove errors in a given set of rawinsonde data. These, or similar schemes, are widely used in diagnostic studies.

e. Comparison techniques

Comparisons of the original and perturbed kinematic fields formed the basis for this study. Although original data were used as the standard, they certainly were not without error. In fact, the introduced perturbations may have negated the effects of originally contained errors at some particular levels and stations. It is believed, however, that the 10 runs, each containing different combinations and magnitudes of perturbations, represent a good sample of situations that can be encountered due to random errors in rawinsonde data.

Both qualitative and quantitative aspects of the perturbed fields were examined. Qualitatively, hand-analyzed spatial fields for each kinematic parameter were subjectively compared with the originals at 850, 700, 500, 300 and 200 mb. This method provides a visual image of the sensitivity of a given parameter when pattern differences are pronounced. A quantitative comparison between the original and 10 perturbed runs also was made for the areas shown in Fig. 1.

For each of the 10 runs of both scales of data, four statistical variables were calculated for each kinematic parameter:

1) The maximum absolute difference between the perturbed and original grid point values.
2) The standard deviation of the differences between the perturbed and original grid point values.
3) The mean absolute deviation of the differences between the perturbed and original grid point values.
4) A linear correlation coefficient between grid points of the two fields (Panofsky and Brier, 1968).

3. Results

a. Relative vorticity

Statistical results of the relative vorticity analysis are given in Table 2. Values of standard, mean and maximum deviation increase with height, with greatest increases occurring at about 500 mb. Indeed, values at 200 mb are two to three times larger than corresponding values at 500 mb. This is to be expected since the input errors (Table 1) were assumed to increase with height. Larger deviations are found at the subsynoptic scale than the synoptic scale due to greater retention of introduced error by the analysis procedures. Correlation coefficients are high from 850–300 mb, ranging from 0.930 to 0.998 (both scales of data). The lowest correlation values, 0.673 (synoptic) and 0.757 (subsynoptic), occur at 200 mb.

At 200 mb, results from the subsynoptic-scale data

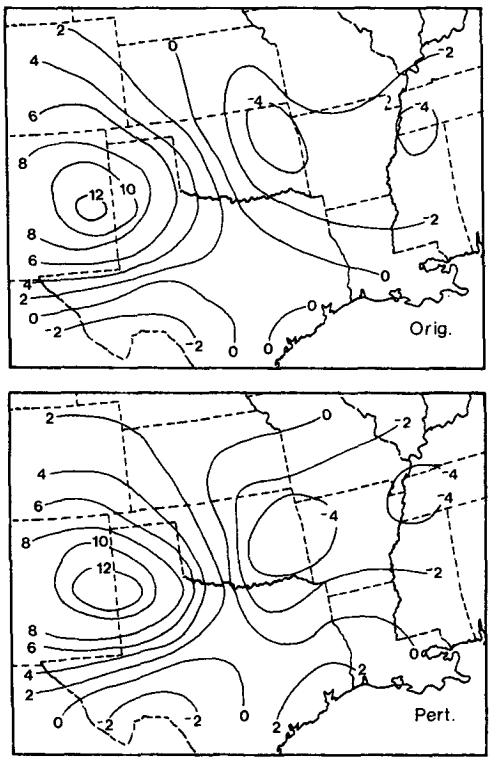

FIG. 4. Spatial fields of relative vorticity (10^{-5} s^{-1}) at 500 mb based on synoptic-scale data. Correlation coefficient for most perturbed field is 0.976.

set exhibit both larger deviation statistics and larger correlations than do results from the synoptic-scale data. Although this may at first seem contradictory, it should be noted that the three deviations and the correlation coefficient describe field comparisons in basically different ways. Larger deviations do correspond to lower correlations at a given data scale; however, additional analyses have shown that the relation between deviations and correlations is not perfectly linear, differs between the two data scales, and varies with altitude. It is not that a particular statistic is right or wrong, but that each views the situation differently. Similar findings will be observed for some of the other parameters as well.

The qualitative discussion on relative vorticity will be limited to a spatial pattern analysis at 500 mb (Fig. 4), the level most often considered by the practicing forecaster. The original synoptic-scale pattern shows a large area of positive relative vorticity centered over eastern New Mexico which is associated with the upper-air trough (Fig. 2). Areas of weak negative relative vorticity occur over the Texas Big Bend area and in a band stretching from eastern Oklahoma to the central Mississippi River Valley. The perturbed field with the poorest correlation (0.976) reveals the insensitivity of relative vorticity to random error; very little change is evident in either pattern or values. The subsynoptic-scale patterns (not shown) show general agreement with those based on synoptic-scale data.

b. Vorticity advection

Vorticity advection appears to be much more affected by random data perturbations than relative vorticity alone. This is quite evident from the statistics shown in Table 3. Again, values for the three deviation quantities increase with height with the greatest increases occurring above 500 mb. Maximum grid point deviations range from 4.9×10^{-10} s^{-2} at 850 mb (synoptic) to 359×10^{-10} s^{-2} at 200 mb (subsynoptic). Notice the significant drop in correlation at the higher levels, particularly the values of 0.208 and 0.321 at 200 mb. This table represents the results of random error in the two "components" of vorticity advection, *viz.*, wind and the gradient of relative vorticity. In order to determine the nature of the sensitivity, three separate analyses were performed. The original field was compared to runs per-

TABLE 3. Statistical data on vorticity advection (10^{-10} s^{-2}). The original field was computed using observed data only while perturbed u, v wind components and perturbed relative vorticity were used for the 10 perturbed fields.

Level (mb)	Data scale	Range of values for the 10 perturbed runs: Maximum deviation	Standard deviation	Mean deviation	Correlation coefficient
850	S	2.3–4.9	0.9–1.7	0.7–1.4	0.962–0.990
	Sub	3.7–7.8	1.7–3.2	1.3–2.6	0.963–0.990
700	S	4.5–12.5	1.8–3.3	1.3–2.6	0.956–0.988
	Sub	11.2–22.1	3.4–7.1	2.7–5.5	0.903–0.977
500	S	11.2–35.0	5.0–10.1	4.1–8.2	0.932–0.983
	Sub	28.9–43.3	9.8–14.9	6.6–12.1	0.888–0.959
300	S	31.9–101.0	10.7–26.3	8.3–19.7	0.853–0.973
	Sub	70.9–181.0	27.8–53.4	22.6–39.5	0.848–0.969
200	S	97.0–230.0	23.1–55.9	16.1–35.3	0.208–0.638
	Sub	138.0–359.0	54.2–109.0	36.8–81.7	0.321–0.775

TABLE 4. Correlation coefficients of vorticity advection (10^{-10} s^{-2}) for runs A, B and C as described in the text.

Level (mb)	Data scale	A	B	C
850	S	0.962–0.990	0.968–0.992	0.986–0.999
	Sub	0.963–0.990	0.955–0.989	0.996–0.999
700	S	0.956–0.988	0.946–0.986	0.993–0.999
	Sub	0.903–0.977	0.902–0.971	0.997–0.998
500	S	0.932–0.983	0.925–0.984	0.992–0.999
	Sub	0.888–0.959	0.862–0.957	0.992–0.998
300	S	0.853–0.973	0.802–0.971	0.979–0.997
	Sub	0.848–0.969	0.815–0.974	0.987–0.996
200	S	0.208–0.638	0.182–0.633	0.981–0.995
	Sub	0.321–0.775	0.291–0.772	0.977–0.993

turbed in the following manner: (A) perturbed winds with perturbed relative vorticity (also in Table 3), (B) original advecting winds with perturbed relative vorticity, and (C) perturbed advecting winds with original relative vorticity. The results, given in Table 4, clearly indicate that the gradient of vorticity (group B), rather than the advecting winds, produce the lower correlations. The problem occurs because we are taking the gradient of an already perturbed quantity which leads to the amplification of short-wave phenomena, whether real or due to data errors. When upper-tropospheric vorticity advection is desired, these results suggest that the vorticity pattern should be computed using a method that is less error prone, such as employing the geostrophic or balance equations.

Fig. 5 shows the original and most perturbed synoptic-scale patterns of vorticity advection at the often-used 500 mb level. ("Most perturbed" in this discussion refers to perturbed winds with perturbed

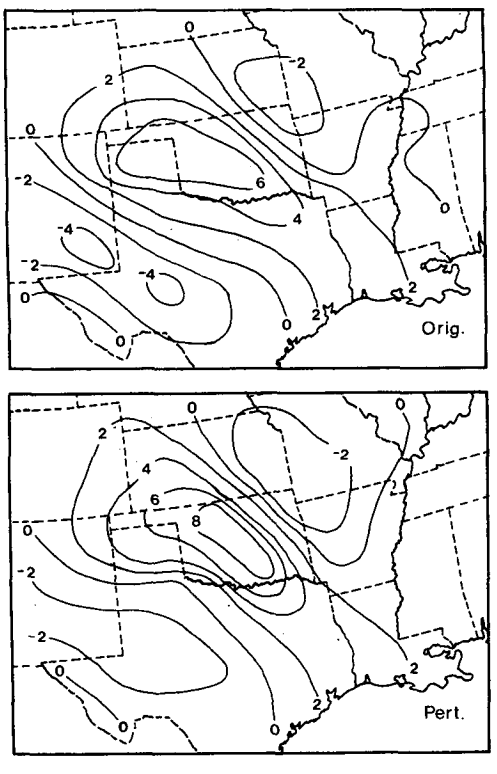

FIG. 5. Spatial fields of vorticity advection (10^{-9} s^{-2}) at 500 mb based on synoptic-scale data. Correlation coefficient for most perturbed field is 0.932.

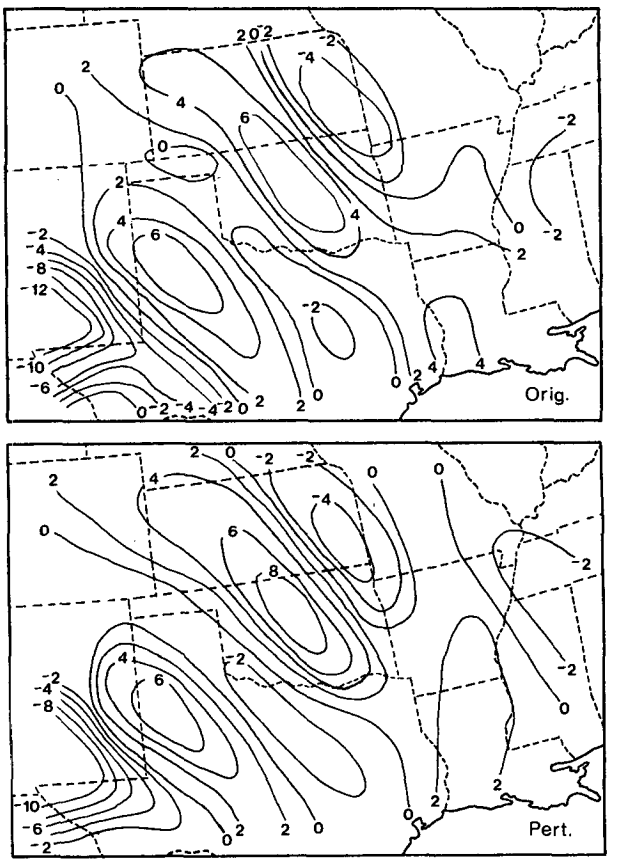

FIG. 6. As in Fig. 5, except based on subsynoptic-scale data. Correlation coefficient for most perturbed field is 0.888.

TABLE 5. Statistical data on adjusted horizontal divergence (10^{-6} s^{-1}) for the original and 10 perturbed fields.

Level (mb)	Data scale	Range of values for the 10 perturbed runs			
		Maximum deviation	Standard deviation	Mean deviation	Correlation coefficient
850	S	4.5–8.8	2.0–3.0	1.6–2.3	0.989–0.994
	Sub	7.2–13.2	2.5–5.0	1.9–4.0	0.973–0.994
700	S	5.6–11.6	2.2–4.7	1.8–3.9	0.944–0.985
	Sub	12.0–20.4	4.4–7.5	3.7–6.1	0.919–0.970
500	S	11.1–25.6	4.2–8.8	3.4–7.1	0.884–0.970
	Sub	16.3–30.7	7.3–11.1	6.1–9.3	0.812–0.921
300	S	19.3–43.9	8.3–15.0	7.0–12.9	0.713–0.933
	Sub	35.2–58.5	14.0–21.1	11.6–17.1	0.794–0.934
200	S	30.2–57.8	11.3–21.5	8.9–17.0	0.425–0.755
	Sub	38.2–111.0	12.6–32.8	9.5–26.8	0.489–0.866

relative vorticity.) Originally, an area of strong positive vorticity advection (PVA) centered over Oklahoma is bordered on the northeast and southwest by areas of weak negative vorticity advection. The major PVA center is closely related to the convective area of 2035 GMT (Fig. 2a). The perturbed field with poorest correlation (0.932) maintains the general pattern, with slightly increasing positive values and decreasing negative values. When subsynoptic-scale data are employed (Fig. 6), the center of PVA is split with an intrusion of negative values extending from southeastern to north central Texas. This feature is apparent in both the original and most perturbed runs. Thus, patterns of vorticity advection are relatively insensitive to errors at 500 mb, but noticeable differences exist between original patterns derived from synoptic- and subsynoptic-scale data. In the southwestern quadrant of the area, some of the contrasts between scales might be due to the comparatively small number of stations available for the objective analysis at the synoptic scale, i.e., few stations are within the scan radii. This is a region of fairly sharp curvature where additional stations would be helpful in defining the flow. As suggested by Table 3, pattern comparisons at 300 and 200 mb are poorer than those at 500 mb; however, vorticity advection at the higher levels is used less frequently.

c. *Horizontal divergence*

Statistics for adjusted divergence (Table 5) again show a general increase with height in deviation values. The correlation coefficients decrease significantly with altitude to a minimum of 0.425 at 200 mb. As observed with the previously mentioned parameters, values of the three deviation parameters are greater at the subsynoptic scale than at the synoptic scale due to added retention of the introduced perturbations. A comparison of Tables 2 and 5 shows that the correlation coefficients for relative vorticity are greater at all levels than those for divergence. This confirms quantitatively a widely mentioned concept of meteorology—accurate computation of divergence is more difficult than accurate computation of vorticity. Since relative vorticity at these scales has a greater magnitude than does divergence, introduced wind perturbations represent a greater percentage error for divergence than for vorticity.

Both lower- and upper-level horizontal divergence are often used in the daily forecasting routine. Fig. 7 shows that at 850 mb, random errors do not greatly

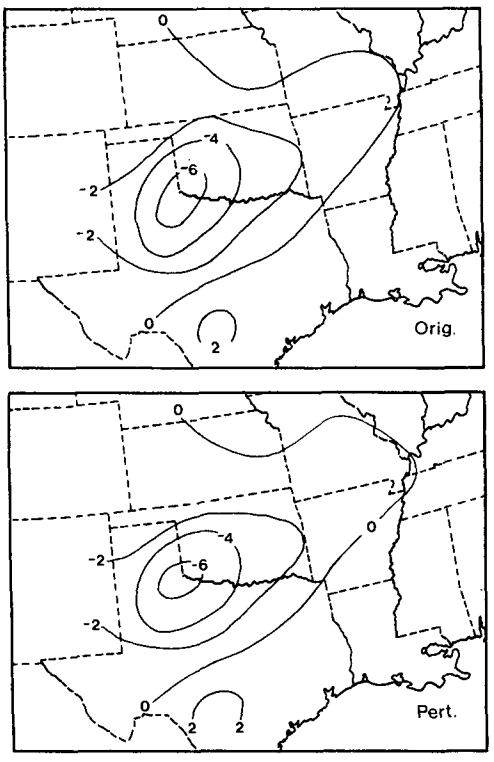

FIG. 7. Spatial fields of horizontal divergence (10^{-5} s^{-1}) at 850 mb based on synoptic-scale data. Correlation coefficient for most perturbed field is 0.989.

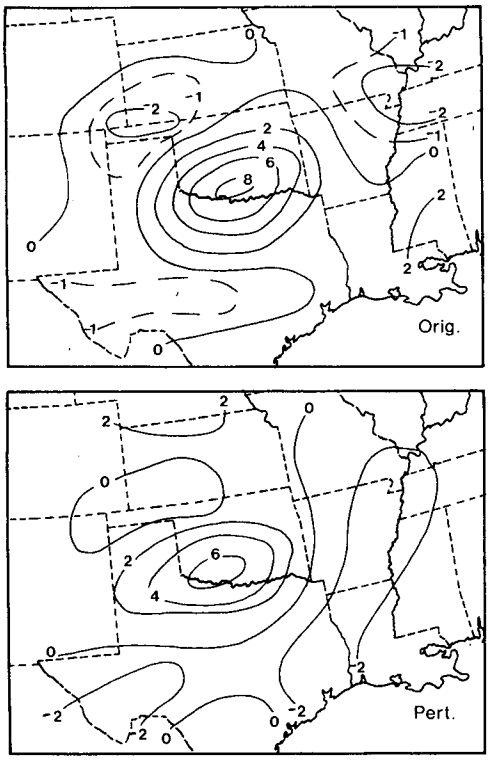

FIG. 8. As in Fig. 7, except at 300 mb. Correlation coefficient for most perturbed field is 0.713.

affect synoptic-scale (or subsynoptic-scale, not shown) fields of horizontal divergence; this agreement corresponds with the high correlation in Table 5. Both the original field and the perturbed field with lowest correlation (0.989) show a well-developed center of convergence over the western Red River Valley. At higher levels, however, the effects of random errors become more pronounced. Fig. 8 gives the synoptic-scale original and "worst" correlation (0.713) fields at 300 mb. The major area of positive divergence centered over the Wichita Falls area and associated with the severe storms (Fig. 2a) also appears in the field having the lowest correlation. However, the area of weak positive values along the Texas-Louisiana border changes sign due to the introduced error. The two fields of upper-level divergence based on subsynoptic-scale data both show the major feature over the Red River Valley (Fig. 9). Central values at the subsynoptic scale are somewhat greater than those based on synoptic-scale data (Fig. 8), but this is not surprising since divergence is scale dependent. Less intense features over the remainder of the area are altered in position and magnitude similar to that seen at the coarser resolution. Although divergence is greatly affected by data errors, it is noteworthy, and somewhat comforting, that such errors do not prohibit the detection of the major upper-level feature associated with the intense convection.

d. Vertical motion

Statistical results obtained for adjusted vertical motion are presented in Table 6. As with the previous kinematic quantities, the deviations increase with height to 300 mb; at 200 mb, however, there is a decrease. This is the result of the O'Brien scheme forcing the vertical motions to zero at 100 mb, a useful procedure for obtaining reasonable vertical motion profiles regardless of random errors which may be present in wind data. Correlations up to 500 mb generally are above 0.95 but decrease noticeably above 500 mb, reflecting the sensitivity of vertical velocities to the accumulation of wind errors in the upward integration process.

Vertical motion at 500 mb is often used in diagnostic and forecasting routines. At the synoptic scale (Fig. 10), both the original and most perturbed (0.946) fields show a major center of upward vertical motion over the Wichita Falls area. Regions of downward motion appear in southwestern Texas and over the middle Mississippi River Valley. This area of ascent agrees with the storm area (Fig. 2) and the patterns of the previously mentioned parameters. Only minor differences in the two patterns are evi-

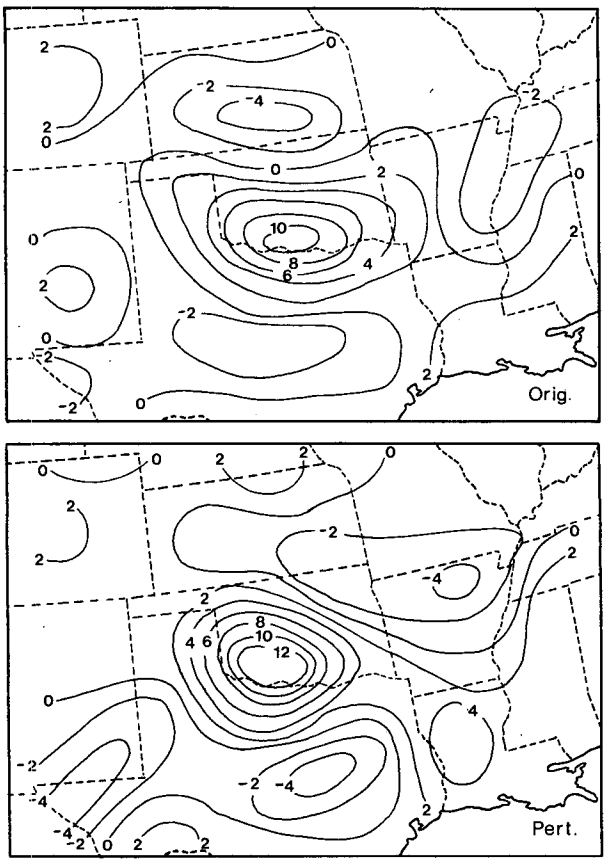

FIG. 9. As in Fig. 8 (300 mb), except based on subsynoptic-scale data. Correlation coefficient for most perturbed field is 0.794.

TABLE 6. Statistical data on adjusted vertical motion ($\mu b\ s^{-1}$) for the original and 10 perturbed fields.

Level (mb)	Data scale	Range of values for the 10 perturbed runs			
		Maximum deviation	Standard deviation	Mean deviation	Correlation coefficient
850	S	0.4–0.7	0.1–0.2	0.1–0.2	0.988–0.994
	Sub	0.7–1.2	0.3–0.4	0.2–0.3	0.981–0.992
700	S	0.7–1.6	0.3–0.5	0.2–0.4	0.987–0.996
	Sub	1.0–2.4	0.4–0.8	0.4–0.6	0.980–0.994
500	S	1.5–3.8	0.6–1.2	0.5–1.0	0.946–0.986
	Sub	2.4–3.8	0.8–1.4	0.6–1.2	0.963–0.988
300	S	2.4–5.2	0.8–1.6	0.7–1.3	0.689–0.911
	Sub	3.1–6.3	1.2–2.3	1.0–1.9	0.685–0.932
200	S	2.1–3.4	0.7–1.3	0.6–1.1	0.489–0.854
	Sub	2.1–5.5	1.0–1.6	0.8–1.3	0.671–0.885

dent. At the subsynoptic scale (Fig. 11), the major centers are similar in location to those at the coarser resolution (Fig. 10); however, some differences between patterns are seen to the north and east of the center. Magnitudes at the finer scale are somewhat greater than those based on synoptic-scale data. Agreement between the original and most perturbed subsynoptic-scale pattern (0.963) is quite good. It is noteworthy that even at levels exhibiting low correlation coefficients [e.g., 0.425 and 0.489 at 200 mb (not shown)] the resulting spatial patterns can be used to infer the major center of upward vertical motion over the Red River Valley.

e. *Temperature advection*

Statistical results of temperature advection, shown in Table 7, indicate high correlation coefficients throughout the atmosphere, *viz.*, ≥ 0.869. Spatial

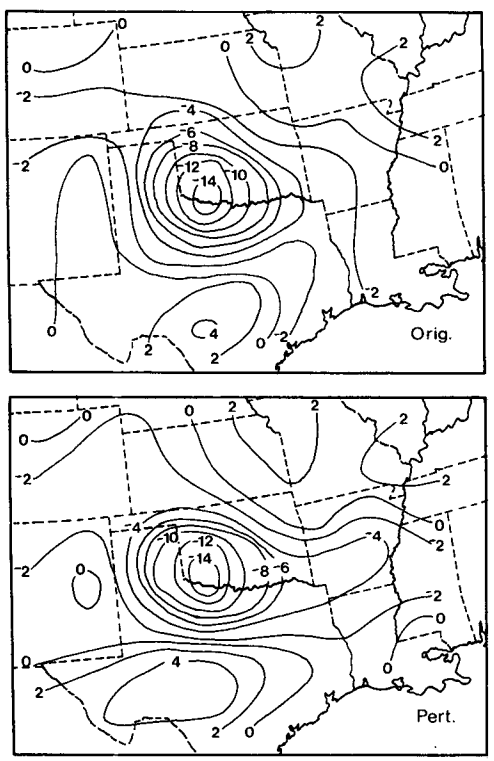

FIG. 10. Spatial fields of vertical motion ($\mu b\ s^{-1}$) at 500 mb based on synoptic-scale data. Correlation coefficient of most perturbed field is 0.946.

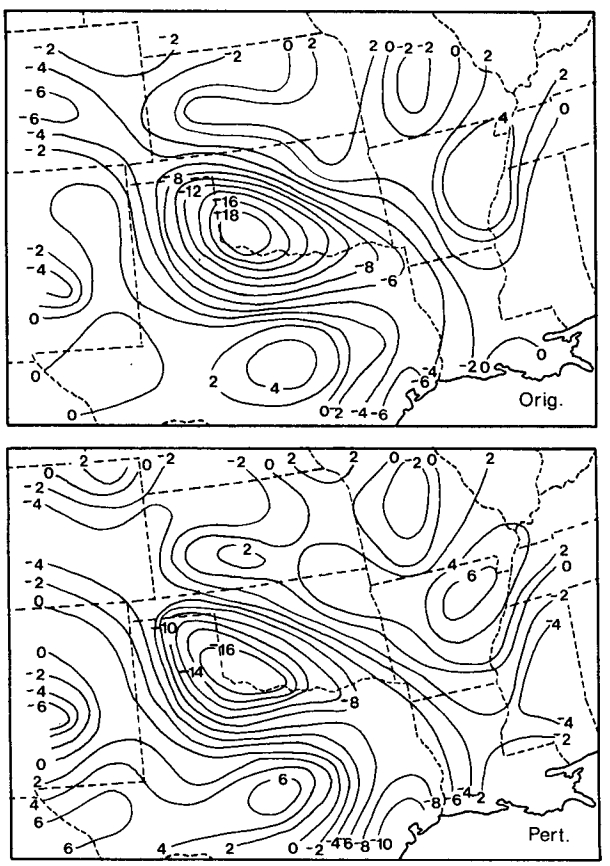

FIG. 11. As in Fig. 10, except based on subsynoptic-scale data. Correlation coefficient for most perturbed field is 0.963.

TABLE 7. Statistical data on temperature advection (10^{-5} °C s^{-1}) for the original and 10 perturbed runs.

Level (mb)	Data scale	Range of values for the 10 perturbed runs			
		Maximum deviation	Standard deviation	Mean deviation	Correlation coefficient
850	S	2.7–7.0	1.0–2.7	0.9–2.3	0.966–0.995
	Sub	3.8–7.4	1.7–2.6	1.1–2.0	0.966–0.985
700	S	3.1–7.0	1.1–2.5	0.9–1.9	0.987–0.997
	Sub	6.3–12.7	2.2–3.8	1.6–3.1	0.963–0.983
500	S	3.1–15.2	1.3–4.0	1.1–2.9	0.952–0.993
	Sub	6.5–16.0	2.5–5.7	2.0–4.3	0.918–0.984
300	S	9.6–14.2	3.5–5.5	2.7–4.7	0.951–0.979
	Sub	12.9–35.1	4.4–8.1	3.5–6.3	0.889–0.962
200	S	10.1–19.2	3.2–6.3	2.6–4.5	0.869–0.967
	Sub	15.3–28.1	4.8–9.9	3.4–7.4	0.961–0.989

fields at every level, and for both scales of data, show that all patterns and values are consistent with one another. In this case, both temperature and its gradient are not as greatly affected by error as was observed with vorticity advection (Table 4).

f. Comparison with a previous study

Table 8 presents a comparison of results between this study and those obtained by Dupuis and Scoggins (1979). The Dupuis and Scoggins study differs from the present in that the error propagation method, which did not allow for smoothing procedures or objective analyses, was used. The assumed errors are similar for both studies (Table 1). The comparison is based on the range of standard deviations which were *computed* for synoptic-scale data in the present study and *predicted* by the Dupuis and Scoggins error equations. With few exceptions, standard deviations for the current random error study are smaller than those from the error propagation study (Dupuis and Scoggins, 1979). This speaks favorably of the use of computational smoothing techniques to reduce the effects of random errors.

TABLE 8. Comparison of standard deviations computed from adjusted synoptic-scale data from the current study and predicted by the Dupuis and Scoggins (1979) study.

Parameter	Level (mb)	Current study	Dupuis and Scoggins
Relative vorticity (10^{-5} s^{-1})	850	0.2 to 0.3	0.5
	700	0.3 to 0.5	1.0
	500	0.4 to 0.9	1.5
	300	0.6 to 1.8	2.2
Vorticity advection (10^{-10} s^{-2})	850	0.9 to 1.7	4.0
	700	1.8 to 3.3	9.0
	500	5.0 to 10.1	16.0
	300	10.7 to 26.3	22.0
Horizontal divergence (10^{-5} s^{-1})	850	0.2 to 0.3	0.5
	700	0.2 to 0.5	1.0
	500	0.4 to 0.9	1.5
	300	0.8 to 1.5	2.2
Vertical motion (μb s^{-1})	850	0.15 to 0.23	0.4
	700	0.3 to 0.5	1.5
	500	0.6 to 1.2	4.0
	300	0.8 to 1.6	7.0
Temperature advection (10^{-5} °C s^{-1})	850	1.0 to 2.7	1.9
	500	1.3 to 4.0	4.5

4. Conclusions

A random error analysis has been performed on data from the AVE-SESAME I experiment to determine the degree of confidence which can be placed on derived kinematic quantities. Both synoptic- and subsynoptic-scale data sets were used to assess sensitivity at the two scales. The data were tested qualitatively as well as quantitatively to ascertain parameter reliability at the levels most often used by the practicing forecaster. The results, based on degree of sensitivity, are as follows:

1) Of the parameters tested, horizontal divergence was found to be the most affected by random errors. Reliability was a function of height; at 850 mb perturbed spatial fields for both scales varied little from the originals, while 300 mb perturbed fields of both data sets contained greater discrepancies with their corresponding originals.

2) Vorticity advection was the next most altered by random error. In this case, effects of wind errors are greater on the gradient of vorticity than on vorticity itself. Perturbed 500 mb spatial patterns, however, were quite acceptable when compared to the original.

3) Vertical motions were most affected by random perturbations at 300 mb and above. Spatial fields at 500 mb, while reflecting some differences between synoptic- and subsynoptic-scale values, maintained good correlation between original and perturbed patterns.

4) As evidenced by both qualitative and quanti-

tative testing, relative vorticity was relatively unaffected by random errors. Spatial patterns at 500 mb were nearly identical for perturbed and original fields.

5) Temperature advection was found to be the least sensitive to random perturbations. Correlation coefficients were consistently high and no significant discrepancies were noted.

An important conclusion is that major kinematic features associated with the Red River Valley outbreak were detectable with perturbed data, even at the higher levels. Weaker features on the periphery of the outbreak area sometimes were distorted, however.

Overall, subsynoptic-scale perturbed data produced greater deviations and, generally, lower correlation coefficients than the synoptic-scale data. While allowing for finer resolution, the smaller scale data apparently permit more random error to pass through the objective analysis schemes. It is noteworthy that fields derived from both the synoptic- and subsynoptic-scale data sets usually revealed the same major kinematic features. Vorticity advection showed the greatest differences between the two scales of resolution. This suggests that, during this particular storm outbreak at least, ordinary synoptic-scale data could describe much of the larger scale atmospheric variability. More detailed analyses, including structure function computations, are underway to explore this facet of the period.

These results are based on one case study when well-defined kinematic patterns, indicating strong forcing, were present. Although a different situation may produce different quantitative results, the general nature of sensitivity should remain the same.

Follow-on studies are underway to better simulate the effects of errors in rawinsonde data. In the current study, the normally distributed wind perturbations (Table 1) were used at all stations regardless of the tracking geometry of the sonde. Because elevation angles vary inversely with wind speed from the surface to the level in question, calculated winds contain greater uncertainty in regions of strong winds than in areas of light winds. Future work will include individual station error statistics that are functions of tracking geometry as well as pressure.

Acknowledgments. The authors thank Mr. Gary Jedlovec for his assistance in data preparation. They also express gratitude to Mr. Paul Meyer for drafting the figures and to Ms. Pat Ryan and Ms. Reeder Wade for typing the manuscript. This work is an extension of a study begun by Captain Emil Berecek while completing requirements for a Master's degree at Saint Louis University. We appreciate suggestions of the anonymous reviewers which helped clarify portions of the text.

The research was sponsored by the National Aeronautics and Space Administration under Contract NAS8-33370 and is under the auspices of the Atmospheric Sciences Division, Space Sciences Laboratory, NASA Marshall Space Flight Center, Alabama. A scholarship from the Air Force Institute of Technology is gratefully acknowledged by Captain Belt.

REFERENCES

Alberty, R. L., D. W. Burgess, C. E. Hane and J. F. Weaver, 1979: Sesame 1979 Operations Summary. NOAA/ERL, Boulder, 253 pp. [Available from NOAA/ERL, RX8, 325 Broadway, Boulder, CO 80303].

Barnes, S. L., 1964: A technique for maximizing detail in numerical weather map analysis. *J. Appl. Meteor.*, **3,** 396–409.

Chen, T. J., and L. F. Bosart, 1977: Quasi-Lagrangian kinetic energy budgets of composite cyclone-anticyclone couplets. *J. Atmos. Sci.*, **34,** 451–464.

Dupuis, S. R., and J. R. Scoggins, 1979: Differences between measured and linearly interpolated synoptic variables over a 12 h period during AVE IV. NASA CR-3150, George C. Marshall Space Flight Center, 131 pp, [Available from Atmospheric Sciences Division, ES-84, Marshall Space Flight Center, AL 35812].

Fuelberg, H. E., and J. R. Scoggins, 1980: Kinetic energy budget during strong jet stream activity over the eastern United States. *Mon. Wea. Rev.*, **108,** 69–77.

Gerhard, M. L., H. E. Fuelberg, S. F. Williams and R. E. Turner, 1979: AVE-SESAME I: 25-mb sounding data. NASA TM-78256, George C. Marshall Space Flight Center, 364 pp. [Available from Atmospheric Sciences Division, ES-84, Marshall Space Flight Center, AL 35812].

Hill, K., G. Wilson and R. Turner, 1979: NASA's participation in the AVE-SESAME '79 program. *Bull. Amer. Meteor. Soc.*, **60,** 1323–1329.

Hodge, M. W., and C. Harmantas, 1965: Compatibility of United States radiosondes. *Mon. Wea. Rev.*, **93,** 253–266.

Kurihara, Y., 1961: Accuracy of winds aloft data and estimation of error in numerical analysis of atmospheric motions. *J. Meteor. Soc. Japan*, **39,** 331–345.

Lenhard, R. W., 1970: Accuracy of radiosonde temperature and pressure height determination. *Bull. Amer. Meteor. Soc.*, **51,** 842–846.

Moore, J. T., and H. E. Fuelberg, 1981: A synoptic analysis of the first AVE-SESAME '79 period. *Bull. Amer. Meteor. Soc.*, **62,** 1577–1590.

O'Brien, J. J., 1970: An alternate solution to the classical vertical velocity problem. *J. Appl. Meteor.* **9,** 197–203.

Panofsky, H. A., and G. W. Brier, 1968: *Some Applications of Statistics to Meteorology.* Pennsylvania State University Press, 224 pp.

Robertson, F. R., and P. J. Smith, 1980: The kinetic energy budgets of two severe storm producing extratropical cyclones. *Mon. Wea. Rev.*, **108,** 127–143.

Shuman F. G., 1957: Numerical methods in weather prediction: II. Smoothing and filtering. *Mon. Wea. Rev.*, **85,** 357–361.

Vincent, D. G., and L. N. Chang, 1975: Kinetic energy budgets of moving systems: Case studies for an extratropical cyclone and hurricane Celia, 1970. *Tellus*, **27,** 215–233.

Ward, J. H., and P. J. Smith, 1976: A kinetic energy budget over North America during a period of short synoptic wave development. *Mon. Wea. Rev.*, **104,** 836–848.